Published in final edited form as:
Biochemistry. 2012 April 3; 51(13): 2819–2828. doi:10.1021/bi2018317.

HIV-1 protease with 20 mutations exhibits extreme resistance to clinical inhibitors through coordinated structural rearrangements

Johnson Agniswamy[a], **Chen-Hsiang Shen**[a], **Annie Aniana**[b], **Jane M. Sayer**[b], **John M. Louis**[b], and **Irene T. Weber**[a,*]

[a]Department of Biology, Molecular Basis of Disease Program, Georgia State University, Atlanta, GA30303

[b]Laboratory of Chemical Physics, National Institute of Diabetes and Digestive and Kidney Diseases, National Institutes of Health, DHHS, Bethesda, Maryland 20892-0520

Abstract

The escape mutant of HIV-1 protease (PR) containing 20 mutations (PR20) undergoes efficient polyprotein processing even in the presence of clinical protease inhibitors (PIs). PR20 shows >3 orders of magnitude decreased affinity for PIs darunavir (DRV) and saquinavir (SQV) relative to PR. Crystal structures of PR20 crystallized with yttrium, substrate analog p2-NC, DRV and SQV reveal three distinct conformations of the flexible flaps and diminished interactions with inhibitors through the combination of multiple mutations. PR20 with yttrium at the active site exhibits widely separated flaps lacking the usual intersubunit contacts seen in other inhibitor-free dimers. Mutations of residues 35–37 in the hinge loop eliminate interactions and perturb the flap conformation. Crystals of PR20/p2-NC contain one uninhibited dimer with one very open flap and one closed flap, and a second inhibitor-bound dimer in the closed form showing six fewer hydrogen bonds with the substrate analog relative to wild type enzyme. PR20 complexes with PIs exhibit expanded S2/S2′ pockets and fewer PI interactions arising from coordinated effects of mutations throughout the structure, in agreement with the strikingly reduced affinity. In particular, insertion of the large aromatic side chains of L10F and L33F alters intersubunit interactions and widens the PI binding site through a network of hydrophobic contacts. The two very open conformations of PR20 as well as the expanded binding site of the inhibitor-bound closed form suggest possible approaches for modifying inhibitors to target extreme drug resistant HIV.

Multi-drug resistance poses a serious challenge in long-term therapy for human immunodeficiency virus (HIV) infection. The HIV protease (PR) plays a crucial role in replication by generating mature infectious viral particles through cleavage of Gag and Gag-Pol polyprotein precursors, and consequently, PR is a highly successful therapeutic target for HIV/AIDS.[1] Therapeutic intervention with the first protease inhibitor (PI) greatly improved the survival of patients infected with HIV, but was followed by rapid emergence of drug resistance.[2–3] Drug resistance develops by selection of “major” mutations within the viral PR gene that decrease binding of the PIs, accompanied by decreased binding of natural

*Corresponding author: Irene T. Weber, Department of Biology, Georgia State University, P.O. Box 4010, Atlanta, GA 30302, USA. iweber@gsu.edu; Phone: 404 413-5411; FAX: 404 413-5301.

Accession codes: The structure coordinates and factors have been deposited in the Protein Data Bank (www.pdb.org) with access codes 3UCB for PR20/DRV, 3UFN for PR20/SQV, 3UHL for PR20/p2-NC and 3UF3 for PR20.

Supporting information available

A second inhibitor is seen bound to PR20 in PR20/DRV and PR20/SQV complexes in addition to the inhibitors bound at the active site. This material is available free of charge via the Internet at http://pubs.acs.org.

substrates and reduced viral replication.[4] The replication of viruses containing major mutations is improved by the compensating effect of "minor" resistance mutations in naturally variable regions[5]. To date, 15 sites for major mutations and 19 for minor mutations have been identified for all nine FDA approved PIs.[6] In addition, drug resistance can develop due to insertion of 1 to 6 amino acids at various sites in the viral PR sequence[7–8] or by mutations in the PR cleavage sites in the Gag precursor.[9]

Mature PR is released by autoproteolysis of the Gag-Pol precursor. It is active as a homodimer of 99-residue subunits in which each subunit contributes one of the two aspartates required for catalysis. Substrate binding is accompanied by a conformational change from an open form that permits substrate entry into the active site cavity to a closed form in which the two flexible flaps (residues 44–57) close down to bind the substrate.[10] Current clinical inhibitors were designed to bind PR with the closed conformation of the flaps. Hence, mutations that affect flap conformation are selected frequently in resistance to PIs and can alter both inhibitor binding and catalytic activity of the enzyme.[6, 10]

We have recently characterized a clinically derived multidrug resistant protease (PR20)[11] bearing 20 mutations (Figure 1)[12], of which 15 are classified as either major or minor drug resistance mutations[6]. Mature PR20 exhibits a dimer dissociation constant (K_d) of ~30 nM, which is >3-fold higher than for PR, and is catalytically competent with a similar turnover rate (k_{cat}) and an approximately 13-fold higher K_m for a synthetic substrate relative to PR (Table S1 in ref. [11]). Relative to PR, PR20 shows a drastically lower affinity for PIs by >3 orders of magnitude. Inhibitor-dissociation constants (K_L) for DRV and SQV binding to PR20 are 41 and 930 nM, respectively, relative to the corresponding K_L values for PR with DRV (0.005–0.01 nM) and SQV (0.4 nM) (Table 1 in ref [11]). Even though the thermal stability of uninhibited PR20 is significantly greater than that of PR, as shown by a 6 °C higher T_m on DSC, consistent with their weak binding, PIs stabilize the ternary complexes of PR20 (dimer+PI) to a significantly lesser extent than when bound to PR. Thus, values of ΔT_m (inhibitor bound minus unbound) are markedly lower for PR20 at 5.3 and 3.1 °C for DRV and SQV, respectively[11] than for PR (22.4 and 19.3 °C)[13].

Autocatalytic cleavage (autoprocessing) of the PR from the viral Gag-Pol precursor polyprotein, particularly at its N terminus, is crucial for its release, viral maturation and propagation. A PR20 precursor analog consisting of PR20 fused at its N-terminus to the 56-amino acid transframe region (TFR), when expressed in *E. coli*, undergoes efficient autoprocessing at the TFR/PR20 site to release mature, catalytically active PR20. Importantly, autoprocessing of TFR-PR20 is unresponsive to inhibition by all clinical PIs in current use.[11] Inhibition is not observed even in the presence of 150–250 μM SQV or DRV, which far exceeds the estimated plasma or intracellular concentration on administration of these drugs in human subjects.[11] In contrast, the IC_{50} for inhibition of wild type TFR-PR autoprocessing by DRV in *E. coli* is 1–2 μM.

These observations indicate that PR20 is a highly evolved drug-resistant mutant and is likely to be clinically unresponsive to all currently available PIs. To examine the structural basis for this extreme drug resistance, we determined the crystal structures of PR20 alone, and bound to DRV and SQV, which fail to block autoprocessing of TFR-PR20, although they are the most effective PIs for inhibition of the wild-type TFR-PR precursor.[11] We also determined the structure of PR20 bound to a substrate analog that mimics the p2-NC natural cleavage site in the Gag-Pol polyprotein in order to assess differences in substrate binding. Three distinct dimeric structures were obtained: a wide open conformation, a semi-open conformation and a closed conformation showing significantly diminished interactions with inhibitors and substrate analog. Comparison of PR20 with wild-type PR structures reveals

the evolving mechanisms in HIV to evade PIs and thus, may lead to improved strategies for targeting extreme multidrug resistant mutants.

Materials and Methods

Construction, Expression and Purification of PR20

A synthetic gene encoding 99 amino acids of the protease derived from the sequence of a clinical isolate[12], termed PR20, was cloned between the Nde1 and BamH1 sites of pET11a vector (Novagen, San Diego, CA) and transformed into *E.coli* BL-21(DE3; Stratagene). Protein expression, purification and folding were carried out as described.[14]

Crystallization

PR20 at 0.25mM concentration was complexed with 1.25mM of DRV, SQV or substrate analog p2-NC at a 1:5 molar ratio and incubated for 30 minutes. All crystallization trials were performed using hanging drop vapor diffusion technique at room temperature. Crystals of the PR20/DRV complex were grown by mixing 1 μl of protein (5 mg/ml) and 1 μl of reservoir solution (1.6M sodium chloride and 0.1M sodium acetate buffer at pH 4.6). Crystals of PR20/SQV were grown with a reservoir solution containing 0.93M sodium chloride and 0.03M citrate-phosphate buffer at pH3.8. The well solution used for growing PR20/p2-NC crystals was 0.9M ammonium sulfate and 0.1M sodium citrate buffer at pH4.5. The PR20 by itself was crystallized with 0.9M sodium chloride, 0.1M yttrium chloride and 0.1m sodium acetate buffer at pH5.5. The crystals were frozen with cryoprotectant containing the respective mother liquor together with 30% glycerol.

X-ray Data Collection and Structure determination

Diffraction data were collected at 100 K on beamline 22-ID of the Southeast Regional Collaborative Access Team (SER-CAT) at the Advanced Photon Source, Argonne National Laboratory. The data were integrated and scaled with HKL2000.[15] The PR20/DRV and PR20 crystal structures were solved by molecular replacement with the wild type HIV-1 PR in complex with DRV (2IEN[16]) as the initial model using PHASER.[17–18] The PR20/SQV crystal structure was solved by molecular replacement with the structure of PR mutant I50V in complex with DRV (2F8G[19]) using MOLREP. The wild type structure in complex with p2-NC (2AOD) was used as the starting model to solve PR20/p2-NC. The 20 mutated residues were pruned to alanine during molecular replacement and the correct amino acid side chain was added during refinement. For PR20/p2-NC structure, the flaps in the model were pruned for successful structure solution and rebuilt during refinement. The PR20/DRV and PR20/SQV structures were refined using SHELX-97, while PR20 was refined with REFMAC 5.2[20] and the model building was carried out in COOT.[21] The lower resolution PR20/p2-NC structure was subjected to several rounds of refinement in REFMAC 5.2[22] with the two dimers as a single TLC group and model building with COOT.[21] The inhibitors were fitted into unambiguous electron density in the three complex structures. Solvent molecules were inserted at stereo chemically reasonable positions using 2Fo-Fc and Fo-Fc maps at 1 and 3 sigma levels, respectively. Molecular figures were prepared with Molscript, Raster3D, and PyMOL (http://www.pymol.org).

Results and Discussion

Crystal Structures of PR20 Exhibit Diverse Flap Conformations

The four crystal structures of PR20 reveal three distinct conformations with remarkable variation in the flaps and shed light on the biophysical and biochemical properties of this resistant mutant (Figure 1A). The diverse flap conformations are well ordered without unusually high B-factors (Figure S1A). The crystal structures were refined to resolutions of

~1.4 to 2.2 Å and R-factors from 16 to 22.5% (Table 1). The free PR20 ($PR20_{open}$), PR20/DRV and PR20/SQV complexes were crystallized with one dimer (residues numbered 1–99 and 1′–99′) in the asymmetric unit. The PR20 crystallized with the p2-NC peptide analog had two dimers per asymmetric unit exhibiting different flap conformations: PR20/p2-NC_{open} has no bound peptide, whereas PR20/p2-NC_{closed} contains the p2-NC analog bound in the active site (Figure S1B). The PR20/p2-NC structure has a high mean B-factor of 46 $Å^2$ compared to values of 21–28 $Å^2$ for the other PR20 structures, probably due to the lower resolution and increased flexibility of the two dimers in the asymmetric unit. The unusual existence of two dimer conformations in the same crystal structure, as well as possible disorder in the individual conformers, may result from weak binding of this substrate analog.

All twenty drug resistant mutations, inhibitors and the p2-NC substrate analog were unambiguously modeled in the structures (see examples in Figure 1B, S1C and S1D). The mutations are distributed broadly around the inhibitor binding site, flaps, flap hinge, dimer interface and regions distal to the active site (Figure 1C and 1D). Four “first shell” mutations D30N, V32I, I47V and I84V alter residues making direct contacts with DRV and SQV inhibitors. Six other mutations Q7K, L10F, L33F, I54L, N88D and L90M are located in the second shell with direct influence on the inhibitor-interacting residues.

PR20 Crystallized with Yttrium Reveals a Wide Open Conformation with No Contact between Flap Tips

PR20 crystallizes in an open conformation in the absence of inhibitor, designated $PR20_{open}$, in the presence of the metal ion yttrium. The inhibitor-free $PR20_{open}$ shows large structural changes in comparison with the free wild type PR (1HHP) as measured by an RMSD value of 1.73 Å for 198 Cα atoms (Figure 2A). The greatest disparity occurs at the flap tips with maximum deviations of >7 Å occurring at Gly49/49′. In the open form of wild type PR, the tips of the two flaps have hydrophobic and hydrophilic interactions with each other. In contrast, the two flaps are completely separated in $PR20_{open}$ exposing a channel where the narrowest constriction of 6.1 Å occurs between the side chain of Ile50 and the carbonyl oxygen of Ile50′. The flap residues 46–54 and 46′–54′ differ in conformation from those of the inhibitor-free wild type PR. This conformation falls into the “open-flap” category described previously [23]. Notably, $PR20_{open}$ most closely resembles the free multidrug resistant mutant named MDR769 (1TW7) containing 9 mutations and the inactivating D25N mutation to prevent self-proteolysis[24], as indicated by the lower RMSD value of 0.61 Å for 198 Cα atoms. The major difference still resides in the flap region with the maximum deviation for Ile50 at the tip of the flap (Figure 2B). The flaps in MDR769 retain intersubunit contacts; the side chains of Ile50/50′ at the tip of both flaps have van der Waals contacts with Pro81′/81 from the opposite monomer, despite the presence of D25N that by itself increases the K_d of wild type PR by two orders of magnitude.[25] In $PR20_{open}$, however, the flap of monomer A has no contact with monomer B since the shortest separation is about 7 Å between Ile50 and Pro81′ (Figure 2B).

Yttrium was identified by very high electron density visible at the active site of the $PR20_{open}$ structure (Figure 2C). The yttrium ion coordinates with three water molecules that form hydrogen bonds with the catalytic Asp25 and 25′. The central water molecule bound to yttrium mimics the central hydroxyl group common to PIs. Various metal ions have been reported to inhibit HIV PR[26] and other crystal structures have metal ions bound at the active site.[27] We considered the possibility that binding of yttrium influences the flap conformation. However, the central yttrium has no direct or water-mediated interaction with flap residues, although a surface layer of water molecules is visible extending from the catalytic aspartate towards flap residue I54L. This water-coordinated yttrium ion resembles the magnesium ion and coordinated water observed in two independent open conformation apo HIV PR structures (2pc0 and 2hb4)[23]. These three structures with magnesium or yttrium

ions have three significantly different open flap conformations, suggesting that the metal binding does not influence the flap conformation in the open form. Since the clinical inhibitors were designed to bind the closed conformation of PR, the water-coordinated yttrium in the open conformation may suggest a novel framework for the design of compounds to combat resistance by targeting the widely separated flaps of multidrug resistant PRs.

Two Unusual Flap Conformations Occur in PR20/p2-NC$_{open}$ Dimer

The open conformation dimer (PR20/p2-NC$_{open}$) has no inhibitor bound at the active site and the flaps have different conformations; flap A is very open, while flap B has a twisted closed form. Similar to PR20$_{open}$, the two flaps in the PR20/p2-NC$_{open}$ dimer have minimal contact with each other with the closest distance of ~4.2 Å occurring between the side chain of Ile50 and Gly51′ (Figure 3A). Moreover, the flaps are 12.2 and 5.4 Å distant from Pro81′/81, respectively, and hence completely lack the intersubunit contacts seen in wild type PR and most mutants. The PR20/p2-NC$_{open}$ dimer differs from the free wild type PR and PR20$_{open}$ showing overall RMSD values of 1.9 and 1.8 Å, respectively, with the largest deviations of over 7 Å occurring at Ile50 and Ile50′. The flap A of PR20/p2-NC$_{open}$ exhibits the most widely open conformation reported for crystal structures of free HIV PRs since the tip shifts by ~4.4 Å relative to PR20$_{open}$ and ~12.2 Å relative to the inhibitor-bound PR20/p2-NC$_{closed}$ (Figure 3B). In contrast, the flap B of PR20/p2-NC$_{open}$ is more similar to the closed form flap in PR20/p2-NC$_{closed}$ (Figure 3B), although the tip of the flap is twisted by ~72° due to the interaction with the flap of a symmetry-related molecule in the crystal lattice. The molecules intertwine so that the two flaps of one dimer occupy the active site cavity of the symmetry-related dimer (Figure S2A).

Superimposition of the PR20$_{open}$, PR20/p2-NC$_{open}$ and PR20/DRV structures reveals a striking variation in flap conformation (Figure 3C and 3D). A combination of lateral and vertical movements separates the flap tips as seen for the PR20$_{open}$ structure relative to the closed form of PR20/DRV. The very open PR20/p2-NC$_{open}$ and PR20$_{open}$ structures show a vertical rise of the flaps away from the catalytic site, which eliminates intersubunit contacts between the flap tips and the 80's loop (Figure 3D). Also, the two flaps separate from each other in the horizontal plane. This variation in flap conformation is presumed to interfere mainly with binding of inhibitors as the PR20 precursor is fully competent for its release[11] and mediating polyprotein processing.[11] Similarly, a recent double electron-electron resonance study showed that polymorphism in HIV-1 PR subtypes can confer altered flap conformation and flexibility.[28]

PR20/p2-NC$_{closed}$ Lacks Significant Interactions with Substrate Analog

PR20/p2-NC$_{closed}$ dimer shows the closed conformation of flaps and diminished interactions with the reduced peptide analog p2-NC. Comparison of PR20/p2-NC$_{closed}$ with the corresponding wild type PR/p2-NC structure[29] reveals significant differences as indicated by an RMSD of 1.1 Å with the maximum deviation of 4.3 Å at the E35D mutation in the hinge loop. PR20 lacks several hydrogen bonds with p2-NC relative to those seen in the wild type complex (Figure 4A and 4B). Notably, the PR20 flaps are missing 3 out of 4 hydrogen bonds connecting the main chain of the substrate analog with Gly48 and 48′ in wild-type PR. In contrast, the MDR769/p2-NC structure shows open flaps lacking all hydrogen bonds with peptide substrate.[30] PR20 has no hydrogen bonds with the side chain of P2′ Gln unlike the three seen in the wild type complex. Also, the side chain of P3′ Arg in PR20/p2-NC$_{closed}$ forms an ion-pair with Asp29 instead of the intersubunit ion pair between Asp29 and Arg8′ in the wild type PR. In PR20, the absence of six hydrogen bonds with the substrate analog is consistent with the 10-fold lower catalytic activity (~ 13x higher K_m) of the mutant and with the presence of a free dimer in the same asymmetric unit. Despite the

markedly diminished interactions of the mature PR20 with this substrate analog, its precursor undergoes autocatalytic processing even in the presence of inhibitors to produce viable virion.[11–12]

Flap Hinge Mutations Perturb Flap Conformation

All the PR20 structures show the same large structural change in the flap hinge region (residues 34 to 43) relative to the corresponding wild-type PR structures, which is attributed in part to the E35D, M36I and S37N mutations (Figure 5A). In fact, residues 31–37 were shown to be critical for the specificity differences between HIV-1 and Simian immunodeficiency virus PRs [31]. In the PR20 structures, the shorter aspartate side chain introduced by the E35D mutation eliminates the ion pair observed between Glu35 and Arg57 at the base of the flap in the wild-type PR, which may affect the monomer stability and increase the variability of PR20 flaps. Further, in the wild-type structures, Met36 interacts with Ile15 and Ile33. All three residues are mutated in PR20 where the M36I mutation causes the loop to rearrange so that the shorter Ile36 side chain maintains hydrophobic contacts with mutated I15V and I33F. This rearrangement is in agreement with the molecular dynamics studies that predict increased flexibility of the flaps due to E35D and M36I mutations.[32–33] Similar twisting of the hinge loop is seen in the crystal structures of HIV-1 PRs from subtype B, subtype F and group N that bear the M36I substitution, despite their different space groups and inhibitors.[14, 34–35] Thus, the hinge loop mutations break the ion pair anchors at the base of the flaps and propagate structural changes to the flap tips. The more variable flaps are expected to influence the monomer-dimer equilibrium and alter the binding of inhibitors as well as the substrates.

PR20/DRV and PR20/SQV Reveal Coordinated Effects of First and Second Shell Mutations

Our high resolution (1.38 and 1.45 Å) structures of PR20 with clinical inhibitors DRV and SQV reveal the coordinated effects of the mutations on the inhibitor binding site. Overall, the two inhibitor complexes are very similar to each other with RMSD value of 0.40 Å for 198 Cα atoms. In contrast, PR20 dimers show larger differences of 1.06 and 0.93 Å, respectively, relative to the corresponding wild-type PR complexes with DRV and SQV (2IEN[16], 3OXC[36]). Similar to the PR20/p2-NC_{closed} complex, the largest deviation of more than 4 Å occurs at the hinge loop. The active site cavity of the PR20/DRV complex is occupied by DRV in two alternate orientations related by a 180° rotation with occupancies of 0.7 and 0.3, while SQV binds in a single conformation. A second inhibitor molecule is seen bound to different sites in the PR20/DRV and PR20/SQV dimers (see SI and Figure S2B), as reported previously for two other PR mutant structures with the same inhibitors.[37–38] The PR20/SQV complex was crystallized at a slightly lower pH (3.8) than the other PR20 complexes (pH of 4.5); however, the conformation of the catalytic aspartates is essentially identical in all PR20 structures. Similarly, the previously published HIV-1 protease single mutant complex of M46L/DRV was crystallized at pH 3.6 with no major conformational change relative to PR/DRV [37].

Unlike the PR20/p2-NC_{closed} complex, PR20 retains the hydrogen bond interactions with SQV and DRV seen for the wild type complexes with minor exceptions. SQV shows a shorter hydrogen bond of 3.1 Å with the carbonyl oxygen of Gly27 compared to a 3.6 Å long interaction in the wild type PR, similar to that described recently in the SQV complex with the L76V single mutant.[39] In the wild type PR, the side chain of Asp30 forms either direct or water mediated hydrogen bond with the P2′ aniline in the major and minor conformations of DRV. In PR20/DRV, however, the Asn side chain of D30N forms a water mediated hydrogen bond with the major conformation of DRV and introduces a new hydrogen bond with the side chain of the N88D mutation in the second shell (Figure 5B). The minor conformation of DRV exhibits a direct hydrogen bond to D30N and no hydrogen

bond forms between the side chains of D30N and N88D. Variations in the interaction of D30N with DRV and N88D were reported for a DRV-resistant clinical isolate.[40] The D30N single mutant does not form a hydrogen bond with Asn88 and resembles the wild-type structure, while D30N in the D30N, N88D double mutant forms a water mediated hydrogen bond with DRV and a direct hydrogen bond with N88D similar to those in the PR20/DRV complex.[41] On the other hand, the conformation of the D30N side chain in PR20/SQV resembles that of the PR/SQV complex and lacks a hydrogen bond with N88D.[6] D30N is the only mutation of a charged first shell residue in PR20 and second shell mutation N88D may compensate for the altered charge. Analysis of mutation patterns in eight thousand and sixty virus isolates reveals that N88D is positively associated with D30N, and facilitates the occurrence of major resistance mutations D30N and L90M resulting in multidrug resistance.[42]

The second shell mutation of L90M exhibits a similar effect in PR20 and single mutant structures.[19, 43] The longer side chain of Met90 forms a shorter C-H…O interaction of 3.4 Å with the carbonyl oxygen of catalytic Asp25 in both monomers compared to the longer van der Waals contact in the wild type PR. These short interactions of L90M disturb the active site at the dimer interface and may contribute to the increased dimer dissociation observed for PR20 relative to PR. The L90M single mutation significantly reduces the dimer stability of PR[43] and increases the catalytic activity.[19, 44] Also, *in vitro* studies show that combining the two mutations D30N and L90M results in PR that exhibits high levels of resistance to nelfinavir[45]. This inhibitor independent mechanism may explain why L90M has been identified as a resistance mutation for all clinical inhibitors except for DRV and TPV.[6]

Mutation L10F acts to perturb the intersubunit ion pairs of Arg8-Asp29′ and Arg8′-Asp29 at the outer edges of the substrate binding site in the closed forms of PR20. Conserved residues Arg8/8′ and Asp29′/29 contribute to the S2/S2′ pockets and form critical interactions with inhibitors. Mutations that eliminate this ion pair produce a temperature sensitive phenotype with altered enzyme activity and thermal stability.[46–47] In the structures of $PR20_{open}$ and the monomer A of PR20/p2-NC_{open} with the open flap, the intersubunit ion pairs of Arg8/8′ and Asp29′/29 exist as usually seen in the open and closed conformations of PR. This ion pair cannot form in PR20/p2-NC_{closed} and in monomer B of PR20/p2-NC_{open} with the closed flap, however, due to rotation of the Arg8/8′ side chain towards mutation Phe10/10′. In the PR20/DRV monomers, the Arg8 side chains exhibit two alternate conformations (0.6 and 0.4 occupancy). The major conformation of the Arg8 side chain rotates to form multiple van der Waals contacts with the edge of the aromatic Phe side chain of L10F, which abolishes the ion pair with Asp29′ and the hydrophobic contacts with DRV (Figure 5C). This rotation of Arg8 away from Asp29′ is prevented in the PR20/SQV complex, since the P2 group of SQV-2 bound at the second site inserts between the side chains of Arg8 and L10F mutation (Figure 5D). Similar interactions of a symmetry related SQV with Arg8′ and Phe10′ occur in the other monomer. Thus, the open flap conformation of PR20 retains the strong intersubunit ion pairs between Arg8/8′ and Asp29′/29, but engagement of substrate or inhibitor can lock down the flaps and eliminate these intersubunit ion pairs, which weakens Arg8/8′ interactions with inhibitors. L10F has a critical role in this reorganization, which is consistent with the identification of L10F as an accessory mutation associated with resistance to several PIs.[6] By serendipity, the PR20/SQV structure reveals a possible mechanism to prevent the L10F-mediated elimination of the intersubunit ion pair by introducing a large hydrophobic group designed to insert between L10F and Arg8.

Multiple Mutations Combine to Expand the S2/S2′ Subsites

The most significant structural changes in the active site cavity occur as an expansion of the S2/S2′ binding sites of the three PR20 inhibitor complexes due to coordinated effects of multiple mutations. First, mutation of four (D30N, V32I, I47V and I84V) of the seven

residues forming the S2/S2′ subsites alters their size, shape and charge. In particular, mutation of Ile47 and Ile84 to smaller residues increases space within the subsites. The distances between the side chain of residues 47 and 84 on opposite sides of the S2/S2′ subsites in the PR20/DRV complex increase by about 2 Å over the corresponding distances in the wild type complex. Similarly, the distances between residues 47 and 84 in PR20/SQV (Figure 5E) and PR20/p2-NC_{closed} complexes expand by ~2–4 Å relative to the wild-type structures revealing a wider S2/S2′ pocket in all PR20 inhibitor complexes.

The expanded S2 and S2′ pockets of PR20/p2-NC_{closed} eliminate two hydrogen bonds of Gly48 and 48′ with p2-NC and permit rotation of the P2′Gln side chain removing three hydrogen bonds with Asp29′ and 30′ seen in wild type PR/p2-NC (Figure 4). In the PR20/SQV complex, the P2′ group of SQV shifts more than 1.5 Å towards the shorter I84′V to compensate for the larger S2′ subsite and maintain interactions with D30N, V32I, I47V and I84V (Figure 5E). The I84V mutation in PR20/SQV eliminates hydrophobic contacts with the P1′ and P1 groups of SQV, similar to the effects of I84V in PR20/DRV and in the single I84V mutant complex.[16] Mutation I47V shows different effects with DRV and SQV. The shorter side chain of Val47 eliminates van der Waals contacts with the P2 group of DRV and with Ile50 that occur in the wild type complex. In the PR20/SQV structure, however, I47V retains the contacts with SQV seen in the PR/SQV. Mutation V32I on the opposite side of the S2/S2′ subsite restores hydrophobic contact with the side chain of I47V, while showing little effect on interactions with inhibitors.

The expanded binding site of PR20 is coupled with the networks of mutations around the inhibitor-binding residues. The interactions formed by second shell residues Thr31 and L33F and 6 distal mutations maintain the main chain of residues 30–32 further from the inhibitor as shown by ~1 Å increased separation between the Cα atoms of residues 32 and 50 in the PR20 inhibitor complexes compared to the equivalent wild type structures. Notably, the large aromatic side chain of L33F protrudes into the hydrophobic core of the protein enhancing hydrophobic contacts to distal mutations of I13V, I15V, M36I and second shell residues Ala22 and Ile85 (Figure 5F). Also, the hydroxyl side chain of Thr31 forms a new hydrogen bond with the hydroxyl side chain introduced by distal mutation L89T (Figure 5F). Mutations of Leu89 are associated with resistance to DRV and TPV.[6] Similarly, the larger L10F side chain adds contacts with Val82 in PR20 (Figure 5C). The hydrophobic contacts of Val82 and Ile85 with L10F and L33F may contribute to the decreased interactions of the 80’s loop with inhibitor and the flaps observed in PR20 complexes. Mutations of remote residues like I13V, I15V, M36I and L89T act to accommodate the larger side chains of mutated Phe10 and Phe33 in the hydrophobic core, and coordinate with second and first shell mutations to expand the inhibitor binding site and decrease hydrophobic contacts with inhibitors.

Implications for drug resistance

The mutations and structural changes in PR20 act to increase its dimer dissociation constant (K_d) by a factor ≥ 30 and reduce the k_{cat}/K_m by ~10-fold, due mainly to a 13-fold increase in K_m relative to wild type PR[11]. These observations are consistent with the enlarged binding site cavity and increased flap mobility in PR20, which may influence binding of substrates and inhibitors. Notably, however, the effects of these factors on inhibitor binding are much larger than the 10-fold decrease in catalytic efficiency for substrate hydrolysis. For example, the binding of PR20 to DRV is 4,000–8,000 times weaker (larger dissociation constant) than that of wild type PR; their precursors also exhibit a similar >250-fold difference in binding affinity to DRV. Consequently, PR20 is not compromised in precursor processing even in the presence of clinical inhibitors, and hence is highly resistant to inhibition by these drugs.

The additional mutations in PR20 compared with the nine in MDR769[24] appear to enhance its resistance to drugs. In comparison with the wild type enzyme, clinical PIs exhibit 1.8 to 590-fold weaker inhibition of MDR769[48], and even weaker binding to PR20[11]. Although PR20 and MDR769[24] exhibit similar twisting of the hinge loop due to the M36I mutation, PR20 bears other mutations in the hinge loop, such as I33F and E35D, that can alter the flexibility of its flaps. Similarly, mutations in the active site cavity of PR20 (D30N, V32I, I47V and I84V) alter the charge and increase the distance between the flaps and the base of the cavity relative to the values in MDR769 (V82A and I84V). Furthermore, PR20 possesses a network of internal mutations (L10F, I13V, I15V, L33F, M36I, N88D and L89T) that restrain the conformation of residues in the inhibitor binding site. It is of interest that responsiveness of PR20 to DRV inhibition is not restored by reverting one or 2 mutant residues to wild type, suggesting that its extreme drug resistance requires the simultaneous selection of multiple mutations.[11]

One approach to overcome multi-drug resistance is the design of PIs to better accommodate the changes induced by mutations, especially the widely separated flaps and expanded S2/S2′ pocket revealed in PR20. The recently reported potent PR inhibitor GRL-0519 with a larger tris-THF moiety as the P2 group compared to the bis-THF group in DRV may provide a good example for further development.[49] Also, drugs with novel interactions with the flaps may be effective to neutralize the changes due to hinge mutations and flap variability. Moreover, the structure of $PR20_{open}$ with yttrium at the active site provides insights for design of drugs that bind the wide open conformation. For example, compounds designed to target the open PR conformation include metallacarboranes and pyrrolidine-based inhibitors.[50–51]

Supplementary Material

Refer to Web version on PubMed Central for supplementary material.

Acknowledgments

Chen-Hsiang Shen was supported in part by the Georgia State University Molecular Basis of Disease Fellowship and the Georgia State University Research Program Enhancement Award in Bioinformatics. This research was authored, in whole or in part, by National Institutes of Health staff. Data were collected at the Southeast Regional Collaborative Access Team (SER-CAT) beamline 22ID at the Advanced Photon Source, Argonne National Laboratory. Supporting institutions may be found at www.ser-cat.org/members.html. DRV and SQV were obtained through the NIH AIDS Research and Reference Reagent Program, Division of AIDS, NIAID, NIH.

Funding: This research was supported, in whole or in part, by the Intramural Research Program of the NIDDK, National Institutes of Health (NIH), Intramural AIDS-Targeted Antiviral Program of the Office of the Director, NIH, and grant GM062920 from the NIH. Use of the Advanced Photon Source was supported by the U. S. Department of Energy, Office of Science, Office of Basic Energy Sciences, under Contract No. W-31-109-Eng-38.

Abbreviations

HIV-1	human immunodeficiency virus type 1
PR	mature HIV-1 protease
PR20	mature HIV-1 protease with 20 mutations
TFR	transframe region
PI	clinical inhibitor of PR
DRV	darunavir
SQV	saquinavir

TPV	tipranavir
DSC	differential scanning calorimetry
RMSD	root mean square deviation

References

1. Kohl NE, Emini EA, Schleif WA, Davis LJ, Heimbach JC, Dixon RA, Scolnick EM, Sigal IS. Active human immunodeficiency virus protease is required for viral infectivity. Proc Natl Acad Sci U S A. 1988; 85:4686–4690. [PubMed: 3290901]
2. Ridky T, Leis J. Development of drug resistance to HIV-1 protease inhibitors. J Biol Chem. 1995; 270:29621–29623. [PubMed: 8530341]
3. Ho DD, Neumann AU, Perelson AS, Chen W, Leonard JM, Markowitz M. Rapid turnover of plasma virions and CD4 lymphocytes in HIV-1 infection. Nature. 1995; 373:123–126. [PubMed: 7816094]
4. Croteau G, Doyon L, Thibeault D, McKercher G, Pilote L, Lamarre D. Impaired fitness of human immunodeficiency virus type 1 variants with high-level resistance to protease inhibitors. J Virol. 1997; 71:1089–1096. [PubMed: 8995629]
5. Mammano F, Trouplin V, Zennou V, Clavel F. Retracing the evolutionary pathways of human immunodeficiency virus type 1 resistance to protease inhibitors: virus fitness in the absence and in the presence of drug. J Virol. 2000; 74:8524–8531. [PubMed: 10954553]
6. Johnson VA, Brun-Vezinet F, Clotet B, Gunthard HF, Kuritzkes DR, Pillay D, Schapiro JM, Richman DD. Update of the Drug Resistance Mutations in HIV-1: December 2010. Top HIV Med. 2010; 18:156–163. [PubMed: 21245516]
7. Winters MA, Merigan TC. Insertions in the human immunodeficiency virus type 1 protease and reverse transcriptase genes: clinical impact and molecular mechanisms. Antimicrob Agents Chemother. 2005; 49:2575–2582. [PubMed: 15980322]
8. Kozisek M, Saskova KG, Rezacova P, Brynda J, van Maarseveen NM, De Jong D, Boucher CA, Kagan RM, Nijhuis M, Konvalinka J. Ninety-nine is not enough: molecular characterization of inhibitor-resistant human immunodeficiency virus type 1 protease mutants with insertions in the flap region. J Virol. 2008; 82:5869–5878. [PubMed: 18400858]
9. Maguire MF, Guinea R, Griffin P, Macmanus S, Elston RC, Wolfram J, Richards N, Hanlon MH, Porter DJ, Wrin T, Parkin N, Tisdale M, Furfine E, Petropoulos C, Snowden BW, Kleim JP. Changes in human immunodeficiency virus type 1 Gag at positions L449 and P453 are linked to I50V protease mutants in vivo and cause reduction of sensitivity to amprenavir and improved viral fitness in vitro. J Virol. 2002; 76:7398–7406. [PubMed: 12097552]
10. Agniswamy J, Weber IT. HIV-1 protease: structural prespectives on drug resistance. Viruses. 2009; 1:1110–1136. [PubMed: 21994585]
11. Louis JM, Aniana A, Weber IT, Sayer JM. Inhibition of autoprocessing of natural variants and multidrug resistant mutant precursors of HIV-1 protease by clinical inhibitors. Proc Natl Acad Sci U S A. 2011; 108:9072–9077. [PubMed: 21576495]
12. Dierynck I, De Wit M, Gustin E, Keuleers I, Vandersmissen J, Hallenberger S, Hertogs K. Binding kinetics of darunavir to human immunodeficiency virus type 1 protease explain the potent antiviral activity and high genetic barrier. J Virol. 2007; 81:13845–13851. [PubMed: 17928344]
13. Sayer JM, Louis JM. Interactions of different inhibitors with active-site aspartyl residues of HIV-1 protease and possible relevance to pepsin. Proteins. 2009; 75:556–568. [PubMed: 18951411]
14. Sayer JM, Agniswamy J, Weber IT, Louis JM. Autocatalytic maturation, physical/chemical properties, and crystal structure of group N HIV-1 protease: relevance to drug resistance. Protein Sci. 2010; 19:2055–2072. [PubMed: 20737578]
15. Otwinowski Z, Minor W. Processing of X-ray diffraction data collected in oscillation mode. Method Enzymol. 1997; 276:307–326.
16. Tie Y, Boross PI, Wang YF, Gaddis L, Hussain AK, Leshchenko S, Ghosh AK, Louis JM, Harrison RW, Weber IT. High resolution crystal structures of HIV-1 protease with a potent non-

peptide inhibitor (UIC-94017) active against multi-drug-resistant clinical strains. J Mol Biol. 2004; 338:341–352. [PubMed: 15066436]

17. McCoy AJ, Grosse-Kunstleve RW, Storoni LC, Read RJ. Likelihood-enhanced fast translation functions. Acta Crystallogr D Biol Crystallogr. 2005; 61:458–464. [PubMed: 15805601]
18. Storoni LC, McCoy AJ, Read RJ. Likelihood-enhanced fast rotation functions. Acta Crystallogr D Biol Crystallogr. 2004; 60:432–438. [PubMed: 14993666]
19. Kovalevsky AY, Tie Y, Liu F, Boross PI, Wang YF, Leshchenko S, Ghosh AK, Harrison RW, Weber IT. Effectiveness of nonpeptide clinical inhibitor TMC-114 on HIV-1 protease with highly drug resistant mutations D30N, I50V, and L90M. J Med Chem. 2006; 49:1379–1387. [PubMed: 16480273]
20. Sheldrick GM, Schneider TR. SHELXL: high-resolution refinement. Methods Enzymol. 1997; 277:319–343. [PubMed: 18488315]
21. Emsley P, Cowtan K. Coot: model-building tools for molecular graphics. Acta Crystallogr D Biol Crystallogr. 2004; 60:2126–2132. [PubMed: 15572765]
22. Murshudov GN, Vagin AA, Dodson EJ. Refinement of macromolecular structures by the maximum-likelihood method. Acta Crystallogr D Biol Crystallogr. 1997; 53:240–255. [PubMed: 15299926]
23. Heaslet H, Rosenfeld R, Giffin M, Lin YC, Tam K, Torbett BE, Elder JH, McRee DE, Stout CD. Conformational flexibility in the flap domains of ligand-free HIV protease. Acta Crystallogr D Biol Crystallogr. 2007; 63:866–875. [PubMed: 17642513]
24. Martin P, Vickrey JF, Proteasa G, Jimenez YL, Wawrzak Z, Winters MA, Merigan TC, Kovari LC. “Wide-open” 1.3 A structure of a multidrug-resistant HIV-1 protease as a drug target. Structure. 2005; 13:1887–1895. [PubMed: 16338417]
25. Sayer JM, Liu F, Ishima R, Weber IT, Louis JM. Effect of the active site D25N mutation on the structure, stability, and ligand binding of the mature HIV-1 protease. J Biol Chem. 2008; 283:13459–13470. [PubMed: 18281688]
26. Woon TC, Brinkworth RI, Fairlie DP. Inhibition of HIV-1 proteinase by metal ions. Int J Biochem. 1992; 24:911–914. [PubMed: 1612181]
27. Wlodawer A, Miller M, Jaskolski M, Sathyanarayana BK, Baldwin E, Weber IT, Selk LM, Clawson L, Schneider J, Kent SB. Conserved folding in retroviral proteases: crystal structure of a synthetic HIV-1 protease. Science. 1989; 245:616–621. [PubMed: 2548279]
28. Kear JL, Blackburn ME, Veloro AM, Dunn BM, Fanucci GE. Subtype polymorphisms among HIV-1 protease variants confer altered flap conformations and flexibility. J Am Chem Soc. 2009; 131:14650–14651. [PubMed: 19788299]
29. Tie Y, Boross PI, Wang YF, Gaddis L, Liu F, Chen X, Tozser J, Harrison RW, Weber IT. Molecular basis for substrate recognition and drug resistance from 1.1 to 1.6 angstroms resolution crystal structures of HIV-1 protease mutants with substrate analogs. FEBS J. 2005; 272:5265–5277. [PubMed: 16218957]
30. Liu Z, Wang Y, Brunzelle J, Kovari IA, Kovari LC. Nine crystal structures determine the substrate envelope of the MDR HIV-1 protease. Protein J. 2011; 30:173–183. [PubMed: 21394574]
31. Swairjo MA, Towler EM, Debouck C, Abdel-Meguid SS. Structural role of the 30’s loop in determining the ligand specificity of the human immunodeficiency virus protease. Biochemistry. 1998; 37:10928–10936. [PubMed: 9692985]
32. Meiselbach H, Horn AH, Harrer T, Sticht H. Insights into amprenavir resistance in E35D HIV-1 protease mutation from molecular dynamics and binding free-energy calculations. J Mol Model. 2007; 13:297–304. [PubMed: 16794810]
33. Ode H, Matsuyama S, Hata M, Neya S, Kakizawa J, Sugiura W, Hoshino T. Computational characterization of structural role of the non-active site mutation M36I of human immunodeficiency virus type 1 protease. J Mol Biol. 2007; 370:598–607. [PubMed: 17524421]
34. Sanches M, Krauchenco S, Martins NH, Gustchina A, Wlodawer A, Polikarpov I. Structural characterization of B and non-B subtypes of HIV-protease: insights into the natural susceptibility to drug resistance development. J Mol Biol. 2007; 369:1029–1040. [PubMed: 17467738]
35. Clemente JC, Moose RE, Hemrajani R, Whitford LR, Govindasamy L, Reutzel R, McKenna R, Agbandje-McKenna M, Goodenow MM, Dunn BM. Comparing the accumulation of active- and

nonactive-site mutations in the HIV-1 protease. Biochemistry. 2004; 43:12141–12151. [PubMed: 15379553]

36. Tie Y, Kovalevsky AY, Boross P, Wang YF, Ghosh AK, Tozser J, Harrison RW, Weber IT. Atomic resolution crystal structures of HIV-1 protease and mutants V82A and I84V with saquinavir. Proteins. 2007; 67:232–242. [PubMed: 17243183]
37. Kovalevsky AY, Liu F, Leshchenko S, Ghosh AK, Louis JM, Harrison RW, Weber IT. Ultra-high resolution crystal structure of HIV-1 protease mutant reveals two binding sites for clinical inhibitor TMC114. J Mol Biol. 2006; 363:161–173. [PubMed: 16962136]
38. Tie Y, Wang YF, Boross PI, Chiu TY, Ghosh AK, Tozser J, Louis JM, Harrison RW, Weber IT. Critical differences in HIV-1 and HIV-2 protease specificity for clinical inhibitors. Protein Sci. 2011; 21:339–350. [PubMed: 22238126]
39. Louis JM, Zhang Y, Sayer JM, Wang YF, Harrison RW, Weber IT. The L76V Drug Resistance Mutation Decreases the Dimer Stability and Rate of Autoprocessing of HIV-1 Protease by Reducing Internal Hydrophobic Contacts. Biochemistry. 2011; 50:4786–4795. [PubMed: 21446746]
40. Saskova KG, Kozisek M, Rezacova P, Brynda J, Yashina T, Kagan RM, Konvalinka J. Molecular characterization of clinical isolates of human immunodeficiency virus resistant to the protease inhibitor darunavir. J Virol. 2009; 83:8810–8818. [PubMed: 19535439]
41. Bandaranayake RM, Kolli M, King NM, Nalivaika EA, Heroux A, Kakizawa J, Sugiura W, Schiffer CA. The effect of clade-specific sequence polymorphisms on HIV-1 protease activity and inhibitor resistance pathways. J Virol. 2010; 84:9995–10003. [PubMed: 20660190]
42. Mitsuya Y, Winters MA, Fessel WJ, Rhee SY, Hurley L, Horberg M, Schiffer CA, Zolopa AR, Shafer RW. N88D facilitates the co-occurrence of D30N and L90M and the development of multidrug resistance in HIV type 1 protease following nelfinavir treatment failure. AIDS Res Hum Retroviruses. 2006; 22:1300–1305. [PubMed: 17209774]
43. Mahalingam B, Wang YF, Boross PI, Tozser J, Louis JM, Harrison RW, Weber IT. Crystal structures of HIV protease V82A and L90M mutants reveal changes in the indinavir-binding site. Eur J Biochem. 2004; 271:1516–1524. [PubMed: 15066177]
44. Shen CH, Wang YF, Kovalevsky AY, Harrison RW, Weber IT. Amprenavir complexes with HIV-1 protease and its drug-resistant mutants altering hydrophobic clusters. FEBS J. 2010; 277:3699–3714. [PubMed: 20695887]
45. Kozisek M, Bray J, Rezacova P, Saskova K, Brynda J, Pokorna J, Mammano F, Rulisek L, Konvalinka J. Molecular analysis of the HIV-1 resistance development: enzymatic activities, crystal structures, and thermodynamics of nelfinavir-resistant HIV protease mutants. J Mol Biol. 2007; 374:1005–1016. [PubMed: 17977555]
46. Mahalingam B, Louis JM, Reed CC, Adomat JM, Krouse J, Wang YF, Harrison RW, Weber IT. Structural and kinetic analysis of drug resistant mutants of HIV-1 protease. Eur J Biochem. 1999; 263:238–245. [PubMed: 10429209]
47. Manchester M, Everitt L, Loeb DD, Hutchison CA 3rd, Swanstrom R. Identification of temperature-sensitive mutants of the human immunodeficiency virus type 1 protease through saturation mutagenesis. Amino acid side chain requirements for temperature sensitivity. J Biol Chem. 1994; 269:7689–7695. [PubMed: 8125995]
48. Wang Y, Liu Z, Brunzelle JS, Kovari IA, Dewdney TG, Reiter SJ, Kovari LC. The higher barrier of darunavir and tipranavir resistance for HIV-1 protease. Biochem Biophys Res Commun. 2011; 412:737–742. [PubMed: 21871444]
49. Ghosh AK, Xu CX, Rao KV, Baldridge A, Agniswamy J, Wang YF, Weber IT, Aoki M, Miguel SG, Amano M, Mitsuya H. Probing multidrug-resistance and protein-ligand interactions with oxatricyclic designed ligands in HIV-1 protease inhibitors. ChemMedChem. 2010; 5:1850–1854. [PubMed: 20827746]
50. Kozisek M, Cigler P, Lepsik M, Fanfrlik J, Rezacova P, Brynda J, Pokorna J, Plesek J, Gruner B, Grantz Saskova K, Vaclavikova J, Kral V, Konvalinka J. Inorganic polyhedral metallacarborane inhibitors of HIV protease: a new approach to overcoming antiviral resistance. J Med Chem. 2008; 51:4839–4843. [PubMed: 18598016]

51. Bottcher J, Blum A, Dorr S, Heine A, Diederich WE, Klebe G. Targeting the open-flap conformation of HIV-1 protease with pyrrolidine-based inhibitors. ChemMedChem. 2008; 3:1337–1344. [PubMed: 18720485]

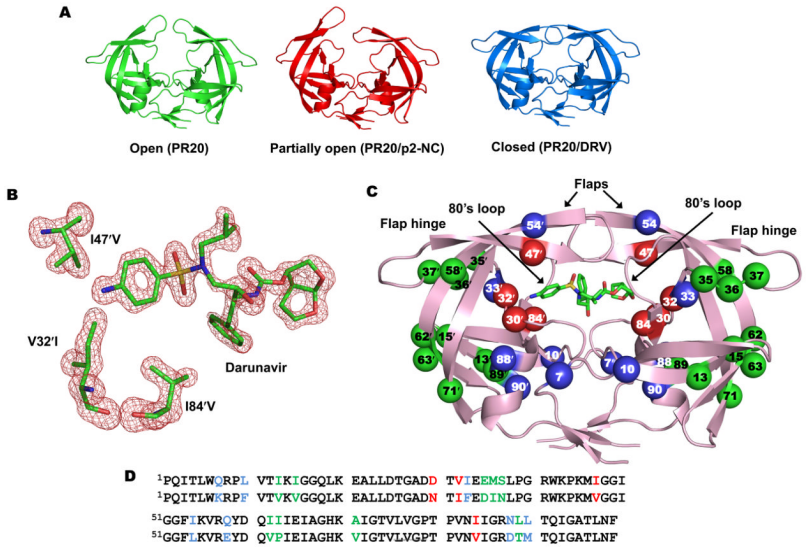

Figure 1.

Crystal structures of PR20 exhibit three different conformations, open, partially open and closed, in the free PR20 and inhibited structures of PR20/p2-NC and PR20/DRV (A). B. F_o-F_c omit map of resistant mutations V32′I, I47′V, I84′ and the major conformation of DRV bound at the active site contoured at 3σ level. C. Sites of the 20 multi drug resistant mutations are mapped on HIV-1 PR (pink cartoon representation) with the bound inhibitor DRV colored with green sticks for carbon atoms. The mutations with direct interaction to inhibitors are colored as red spheres, while second shell mutations are shown as blue spheres, and more distal mutations are shown as green spheres. D. Amino acid sequence of HIV-1 PR (upper line) and PR20 (lower line). The residues are colored similar to panel C. Note that the PR20 sequence includes Q7K, and PR used for comparison in this study includes Q7K, L33I and L63I to prevent autoproteolysis and both include C67A and C95A to eliminate cysteine-induced aggregation.

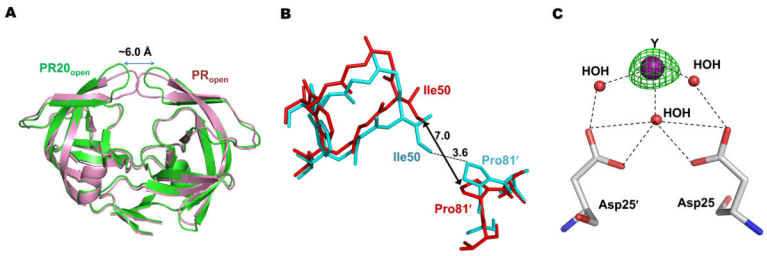

Figure 2.

PR20 has an open conformation in the absence of inhibitor. A. Superposition of free $PR20_{open}$ dimer in cartoon (green) and wild-type PR_{open} dimer (pink) showing a 6.0 Å separation between the flaps of $PR20_{open}$. B. Comparison of Flap A interaction with 80's loop in monomer B between $PR20_{open}$ (red) and MDR 769 (cyan). $PR20_{open}$ has no flap contacts to monomer B. C. F_o-F_c omit map (green contours) of yttrium (magenta) bound at the active site of $PR20_{open}$ contoured at 12σ level. The hydrogen bond interactions are indicated by dashed lines.

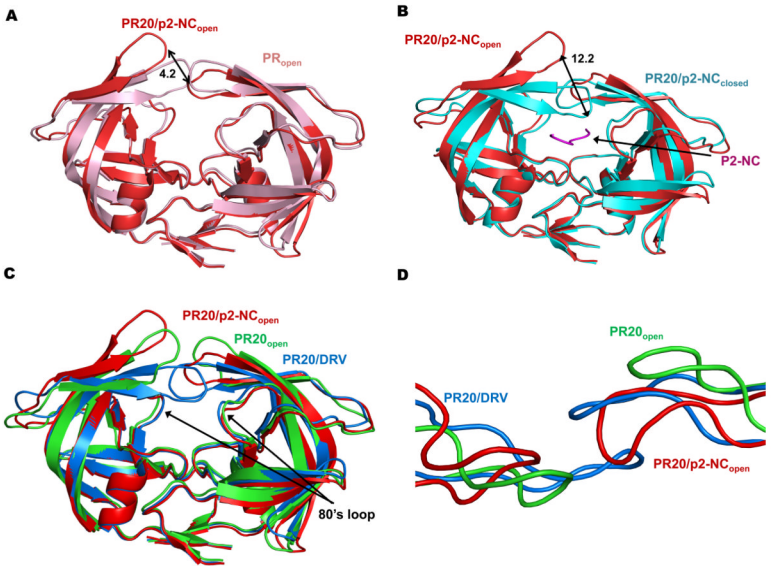

Figure 3.

The conformation of the flaps varies in the PR20 structures. A. Comparison of PR20/p2-NC$_{open}$ (red) with wild-type PR$_{open}$ (pink). The closest distance between the two flaps of PR20/p2-NC$_{open}$ is 4.0 Å. B. Comparison PR20/p2-NC$_{open}$ (red) with PR20/ p2-NC$_{closed}$ (cyan) with the bound p2-NC molecule in PR20/ p2-NC$_{closed}$ complex shown in magenta. The flap A position of PR20/p2-NC$_{open}$ and PR20/ p2-NC$_{closed}$ deviates by a maximum of 12.2 Å. C. Superimposition of PR20$_{open}$ (green), PR20/p2-NC$_{open}$ (red) and PR20/DRV (blue) shown in cartoon. D. The close up of flaps of PR20$_{open}$ (green), PR20/p2-NC$_{open}$ (red) and PR20/DRV (blue) orthogonal to the view in 3C. The flap B of PR20/p2-NC$_{open}$ is curled at the tip in relation to the closed flap B of PR20/DRV.

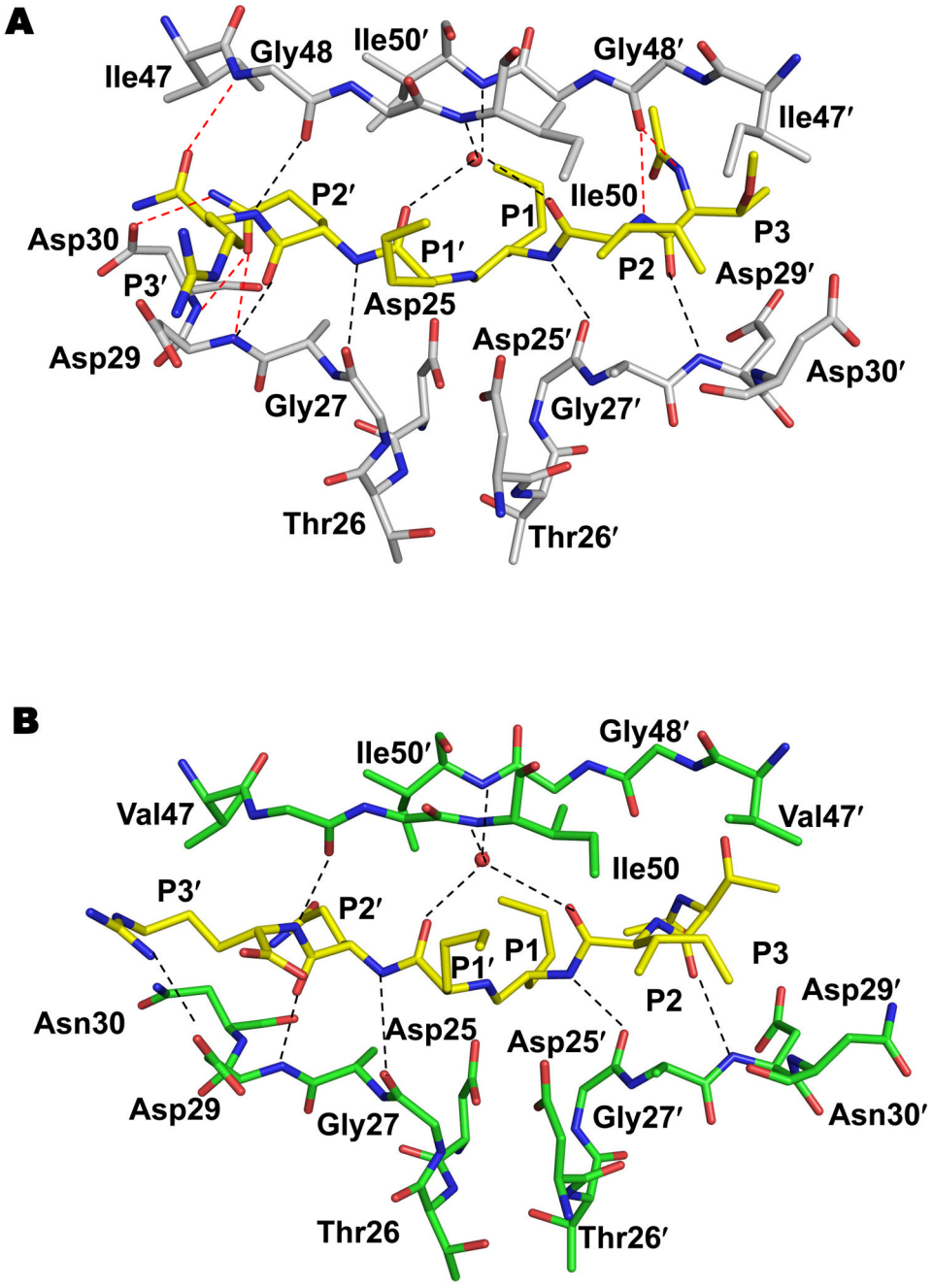

Figure 4.

The hydrogen bond interactions of p2-NC substrate analog with (A) PR and (B) PR20. PR is shown with grey carbons, PR20 with green carbons, and p2-NC is colored with yellow carbons. The p2-NC analog comprises residues P3-P3′, which lie in subsites S3-S3′ of the substrate-binding cavity, with the non-hydrolyzable reduced peptide bond between norleucine at P1 and P1′. The hydrogen bonds are represented in dashed line and the red dashed lines indicate the hydrogen bonds in PR/p2-NC that are absent in PR20/p2-NC_{closed}.

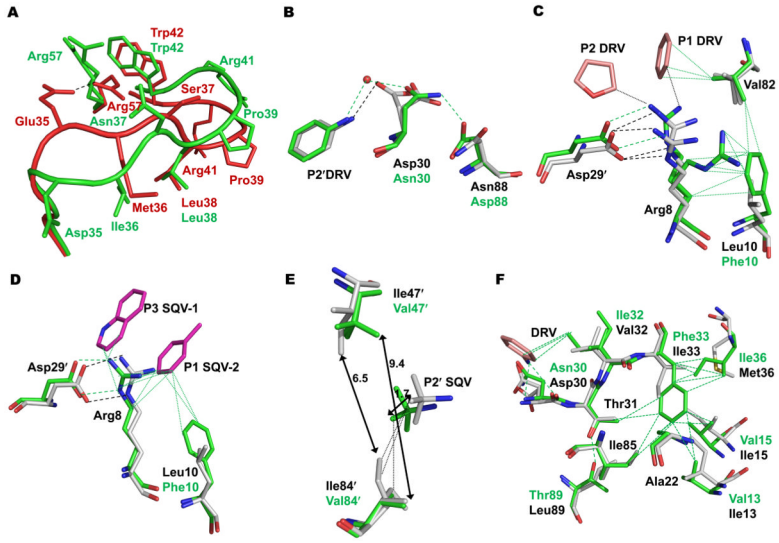

Figure 5.

Comparison of PR20 and wild type PR reveals structural rearrangements associated with mutations. A. Structural changes in the flap hinge region of PR20/DRV (green) complex in comparison to PR/DRV complex (red). B. The direct hydrogen bond between Asp30 and DRV in the wild type complex (grey) is replaced in PR20/DRV (green) by a water mediated interaction between D30N and the major conformation of DRV and a hydrogen bond interaction with N88D. C. L10F mutation disrupts the intersubunit ion pair between the major conformation of Arg8 and Asp29′ in both the monomers of PR20/DRV (green) due to rotation of the guanidinium group of Arg8. PR/DRV is shown in grey carbons and DRV groups in red bonds. D. In PR20/SQV, the P1 group of SQV-2 inserts between Arg8 and L10F and prevents the movement of Arg8. PR20 is shown in green with SQV in magenta. E. I47′V and I84′V mutations in PR20/SQV widen the S2′ pocket by more than 2 Å. F. The L33F mutation connects the active site with the hydrophobic core by hydrophobic interactions indicated by dotted lines. The L89T mutation forms a new hydrogen bond with the hydroxyl of Thr31 which lies between the inhibitor interacting mutations D30N and I32V. Colors as in C.

Table 1

Crystallographic data collection and refinement statistics.

	PR20/DRV	PR20/p2-NC	PR20	PR20/SQV
Space group	$P2_12_12_1$	$P4_32_12$	$P2_12_12_1$	$P2_12_12_1$
Cell Dimensions				
a (Å)	28.64	63.79	44.34	28.83
b (Å)	65.67	63.79	45.85	66.26
c (Å)	94.03	213.66	103.99	93.17
Resolution range	50.0 – 1.38	50.0 – 2.2	50.0 – 1.65	50.0 – 1.45
Total observations	213451	156472	166031	175446
Unique reflections	35869	23454	25386	31978
Redundancy	6.0 (3.2)	6.7 (5.0)	6.5 (3.2)	
Completeness	95.8 (72.0)[a]	99.6 (98.2)	93.9 (61.7)	99.0 (95.4)
$<I/\sigma(I)>$	27.3 (2.6)	24.7 (5.6)	31.9 (2.3)	9.9 (3.2)
R_{sym} (%)	5.4 (38.0)	7.1 (28.2)	5.1 (41.8)	11.6 (33.8)
Refinement resolution range	10 – 1.38	47.5-2.2	10.0 – 1.63	10-1.45
R_{cryst} (%)	16.2	22.4	18.8	17.6
R_{free} (%)	22.3	29.3	22.2	22.5
Number of solvent	108	106	166	130
Mean B-factor ($Å^2$)	27.9	46.1	27.3	20.9
Mean B-factor of the ligand ($Å^2$)	17.5	54.6		12.5
RMS deviations from ideality				
Bond length (Å)	0.01	0.02	0.03	0.01
Angles	0.03 (Å)[b]	1.9 (°)[c]	2.1 (°)[c]	0.03 (Å)[b]

[a] Values in parentheses are given for the highest resolution shell

[b] The angle rmsd in SHELX97 is indicated by distance in Å

[c] The angle rmsd in REFMAC 5.2 is indicated by angle in degrees